coatings

MDPI

Article

Effects of WC on the Microstructure, Wear and Corrosion Resistance of Laser-Deposited CoCrFeNi High Entropy Alloy Coatings

Tao Wu [1,2], Yunxiang Chen [1], Bo Lin [1], Litao Yu [1], Wanyuan Gui [2,*], Jiheng Li [3], Yuan Wu [3] and Dawen Zeng [4]

1 Zhejiang Institute of Mechanical & Electrical Engineering, Hangzhou 310053, China; wutao@zime.edu.cn (T.W.); chyx-zy@163.com (Y.C.); zjfoundry008@163.com (B.L.); t812795407@sina.com (L.Y.)
2 National Center for Materials Service Safety, University of Science and Technology Beijing, Beijing 100083, China
3 State Key Laboratory of Advanced Metals and Materials, University of Science and Technology Beijing, Beijing 100083, China; lijh@ustb.edu.cn (J.L.); wuyuan@ustb.edu.cn (Y.W.)
4 State Key Laboratory of Materials Processing and Die & Mould Technology, Huazhong University of Science and Technology, Wuhan 430074, China; dwzeng@mail.hust.edu.cn
* Correspondence: guiwy@ustb.edu.cn

Abstract: Wear and corrosion resistant properties of high entropy alloy coatings (HEAC) on H13 steel are of particular interest for industrial applications. The CoCrFeNi HEA/WC composite coatings (HEACC) developed in this study were successfully prepared by incorporating 10–40 wt.% WC into a matrix of CoCrFeNi HEA using laser cladding on an H13 steel substrate. Phase transformation, microstructure evolution, microhardness, wear and corrosion resistance of CoCrFeNi HEACC were investigated. According to the results, all CoCrFeNi HEACC exhibited higher wear and corrosion resistance than the H13 steel substrate. Wear resistance of CoCrFeNi HEACC first increases and then decreases with an increase in the concentration of WC particles, and the lowest coefficient of friction and the shallowest depth of wear groove were observed after adding 30 wt.%. Grain refinement strengthening and second-phase particle strengthening may contribute to enhanced hardness and wear resistance of coatings with WC additions. In addition, all the CoCrFeNi HEACC exhibited improved corrosion resistance. In particular, an addition of 10 wt.% WC helped to significantly improve the corrosion resistance and ease of passivation of CoCrFeNi HEACC.

Keywords: CoCrFeNi high entropy alloy; laser cladding; composite coatings; wear resistance; corrosion resistance

check for updates

Citation: Wu, T.; Chen, Y.; Lin, B.; Yu, L.; Gui, W.; Li, J.; Wu, Y.; Zeng, D. Effects of WC on the Microstructure, Wear and Corrosion Resistance of Laser-Deposited CoCrFeNi High Entropy Alloy Coatings. *Coatings* **2022**, *12*, 985. https://doi.org/10.3390/coatings12070985

Academic Editor: Hideyuki Murakami

Received: 18 May 2022
Accepted: 10 July 2022
Published: 12 July 2022

Publisher's Note: MDPI stays neutral with regard to jurisdictional claims in published maps and institutional affiliations.

Copyright: © 2022 by the authors. Licensee MDPI, Basel, Switzerland. This article is an open access article distributed under the terms and conditions of the Creative Commons Attribution (CC BY) license (https://creativecommons.org/licenses/by/4.0/).

1. Introduction

Due to its convenient design of alloying elements, H13 steel is well-established in various parts of the world for use as a hot-work steel that offers high hot strength, plasticity, toughness, and oxidation resistance [1,2]. Nevertheless, the inadequate wear and corrosion resistance of conventional H13 steel reduces the service life of tools after hot working. A surface modification of these components is highly desirable in order to extend their service life as well as prevent premature failure under extreme working conditions [3]. Among the various techniques of surface modification, laser cladding of H13 tool steel with different kinds of materials has recently attracted considerable interest [4–6]. By redesigning the coaxial powder feeding nozzle, the laser cladding technique exhibits more efficient coupling between the laser beam and the powder flow than the traditional laser cladding technique. As a result, the powder particles can be heated to melt before they are poured into the molten pool. Using a limited energy transmission, a micro-molten pool could be formed on the substrate, resulting in coatings with low dilution ratios and excellent metallurgical

bonding, as well as excellent combinations of physical and chemical properties in coatings prepared by the laser cladding technique [7,8].

High entropy alloy (HEA) is gaining significant attention in the engineering coatings industry because of its outstanding strength and hardness, wear and corrosion resistance, and resistance to high temperature softening [9,10]. In recent years, laser cladding has been used to coat steel surfaces with HEA to improve wear resistance and corrosion resistance [11–15]. Different elements perform different functions in HEA [16]. BCC solid solutions are prone to forming when Al, Ti, and Mo are present in HEA. In contrast, FCC solid solutions can be formed by Cu, Co, and Ni in HEA [17–25]. The addition of Co, however, enhances the HEA's plasticity and wear resistance. Ni helps alloys to improve the corrosion resistance and high temperature oxidation resistance of HEA. Recently, much research had been carried out on various CrCoFeNi HEA [19–21,25–32]. Most of these CrCoFeNi HEA were designed through the addition of Mn, Cu, Ti and B elements to enhance hardness, high-temperature oxidation resistance and corrosion resistance. However, the improvement in wear and corrosion resistance achieved through alloying elements is insufficient to enable the wide spread application of CoCrFeNi HEA. The development of a simple and effective method that can significantly improve the wear and corrosion resistance of the CoCrFeNi HEA is therefore necessary.

High entropy alloy coatings (HEAC) prepared by laser cladding have been improved in terms of wear and corrosion resistance by using solid-solution strengthening, fine grain strengthening, and dispersion strengthening. As a promising solid-solution strengthening second phase in HEAC, WC has been considered an ideal choice due to its high melting point (2870 °C), high microhardness (24 GPa), low expansion coefficient (6.9×10^{-6}/K), and slow corrosion rate [33]. As a bonding phase in composite coatings, HEA has properties such as inhibiting the growth of ceramic grains, improving corrosion resistance and oxidation resistance, or jointly improving strength, hardness and toughness. As a result, an HEA/WC composite exhibits superior mechanical properties, corrosion resistance and wear resistance compared to traditional materials [27,28,31,32]. Wei L et al. [34] prepared a CrMnFeCoNi/WC composite using laser cladding. In the presence of $Cr_{23}C_6$, the nucleation of grains was promoted and the expansion of slip bands was hampered. The tensile strength of the composite was considerably higher than that of the single alloy WC composite. Using laser cladding technology, Li, D.Y. et al. [35] applied an HEA/WC composite coating to 304 stainless steel. As a result of the use of laser cladding technology, an HEA coating was deposited onto a stainless steel matrix, and the addition of WC particles was completely decomposed. In the absence of WC, the HEA coating displayed a eutectic structure with alternate growth of BCC and Laves phases. With the addition of WC, an intermetallic compound of NbC was formed and the eutectic structure gradually dissociated. The dissociation tendency increased with the addition of WC. The eutectic structure disappeared completely at 25% WC mass, and the Laves phase grew and aggregated. It is apparent that the addition of WC not only provides a simple composite with HEA as a strengthening phase, but also affects the generation of the HEA phase, resulting in the microstructure formation process of composite materials [36–38].

In this work, we explore a novel CoCrFeNi HEA/WC composite coating (HEACC) prepared by laser cladding through mixing 10~40 wt.% WC particles into a CoCrFeNi HEA matrix. Interestingly, the microstructure and wear and corrosion resistance of HEACC simultaneously change significantly with increasing the mass of the WC particles' addition. Moreover, the possible factors contributing to the increased wear and corrosion resistance are proposed and discussed in detail.

2. Experimental Section

2.1. Materials Preparation and Coating Deposition

H13 steel was used as the test substrate, and the substrate size was 200 mm × 200 mm × 20 mm. The substrate was polished with SiC sandpaper (No. 400) before the clad in order to remove oxide scales and ensure certain surface roughness in order to improve

the bonding between the cladding layer and the substrate. Ethanol was used to remove grease from the surface of the substrate and to dry it. The high entropy alloy powder (Vilory Advanced Materials Technology Co., Ltd., Xuzhou, China) used in this work was prepared by true air atomization with powder sizes ranging from 45–105 µm (Table 1); the chemical composition of CoCrFeNi HEA powder is presented in Table 2. Commercial sintered broken WC powder (QM-3SP2 Planetary ball mill, Changsha Deco Instrument Equipment Co., Ltd., Changsha, China) with the mass ratios of of 10%, 20%, 30% and 40% were mixed with CoCrFeNi HEA powder by ball milling with 120 rpm in a ball crusher for 8 h (ball-to-powder weight ratio 3:1) and were then dried 2 h in an oven (80 °C).

Table 1. Particle size distribution of CoCrFeNi HEA powder.

D10/µm	D50/µm	D90/µm
46.9	71.9	110

Table 2. The chemical composition of CoCrFeNi HEAs powder (wt.%).

Co	Cr	Fe	Ni	O/ppm	N/ppm
Bal.	23.19	25.96	26.45	370	170

The coaxial powder feeding method of laser cladding was adopted (Figure 1) to clad the mixed powder. A high-purity argon gas (99.9%) was used as a protective gas. The laser was an LDF-4000 semiconductor laser made by Laserline (Mülheim-Kärlich, Germany), with a spot diameter of 3 mm, a laser power of 1500 W, and a scanning speed of 8 mm/s. There was a 40% overlap between the multi-channels and the multi-channels were clad in one layer. The cladding area was 30 mm × 30 mm, and the coating thickness was 1 mm. The process parameters are presented in Table 3.

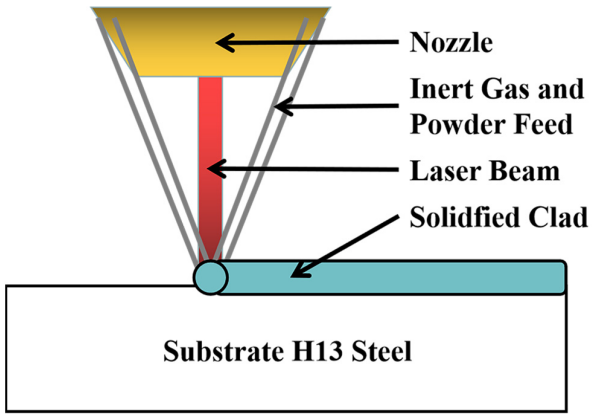

Figure 1. Schematic diagram of laser cladding process.

Table 3. Multiple variations in processing parameters of coatings.

Power (w)	Spot Diameter (mm)	Welding Speed (mm/s)	Lap Ratio (%)	Flow Rate (L·min^{-1})
1500	3.0	10.0/8.0	40	15

2.2. Characterization

The morphology of the mixed powders and laser cladding composite coatings was characterized by field emission scanning electron microscopy (FESEM, Zeiss Supra 55, Carl Zeiss AG, Oberkochen, Germany). EDS was used to characterize the element distribution of the sample. To enhance the EDS precision for quantification, the take-off angle was 36.5° and the live time was 2 min. The phase characterization of powders and coatings was

conducted using X-ray diffraction (XRD, Panalytical X-pert Pro, PANalytical B.V., Alemlo, The Netherlands), operating at a voltage of 40 kV at room temperature, a tube current of 40 mA, and a scanning rate of 10°/min. At the point of emission of the X-ray, the slit width is 10 mm × 10 mm, and at the point of reception of the X-ray, it is 8 mm × 20 mm. The friction and wear properties of the coating were determined using a BRUKER UMT-Tribolab friction and wear tester. The grinding head was made of Si_3N_4, the load was 8 N, the frequency was 5.0 Hz, the friction stroke was 1 cm, the test time was 30 min, and the wear weight loss was measured by a high-precision analytical balance. The electrochemical measurements were taken using a three-electrode system (CHI660E, Huachen Instrument Ltd., Shanghai, China) with an immersion area of approximately 1 cm^2 and a working electrode for testing the coating. The reference electrode for the electrode metal platinum sheet was Ag-AgCl (saturated KCl). A 3.5 wt.% NaCl solution was selected as the electrolyte. Before the electrochemical test, samples were soaked in the electrolyte until the stable open-circuit potential was reached (about 600 s). A potential sweep rate of 1 mV/s was used to record potentiodynamic polarization curves in the air. In order to obtain a polarization curve with good repeatability, all specimens were measured at ambient temperature for at least three successive measurements.

3. Results and Discussion

3.1. Phase Composition and Microstructure Feature

Figure 2 presents the FESEM images of the CoCrFeNi HEA powder and the effect of the WC content on the surface morphology of the CoCrFeNi HEA powder after mechanical mixing. Figure 2a shows that the CoCrFeNi HEA powder mainly consists of spherical particles with a particle size between 45–105 μm and uniform distribution. The local enlargement of Figure 2a shows that some particles are adhering or deforming in the vicinity of their contact with grinding balls as well as collisions between particles, due to CoCrFeNi HEA's excellent plastic and moderation hardness [39]. Therefore, the particle is deformed by external forces, thereby affecting the particle's sphericity. As the WC particle mass increases from 10 to 40 wt.% (Figure 2b,e), some floccules and irregular particles appear and increase in number on the surface of the CoCrFeNi HEA powder. Because WC particles are prepared by a combination of sistering and broken powder methods, their sphericity is poor and most of them have irregular shapes. In addition, EDS analysis was conducted on irregular WC particles, as shown in Figure 2f. Carbon element ratio to tungsten element was W_3C_7, which means that part of the tungsten element was lost during the mechanical mixing process.

Figure 3 illustrates XRD patterns of powder after mechanical mixing and laser cladding. As illustrated by Figure 3a, CoCrFeNi HEA powder is characterized by a single-phase FCC structure. When WC particles are added to mechanical ball mills and are mixed over a long period of time, a small number of compounds are produced. The CoCrFeNi HEACC is formed by laser cladding and consists of FCC structure, WC, and some intermetallic compounds, as shown in Figure 3b. We can infer that some WC decomposes during laser cladding and some intermetallic compounds precipitate in the face-centered cubic matrix.

In order to investigate the influence of WC addition on the lattice structure of CoCrFeNi HEACC, we calculated the crystal size D and lattice constant an using the Scheler formula and Bragg Equation [40,41]. The corresponding results are shown in Table 3.

$$\mathrm{D} = \frac{0.89\lambda}{B\cos\theta} \tag{1}$$

$$\mathrm{a} = d_{hkl} \bullet \sqrt{h^2 + k^2 + l^2}. \tag{2}$$

The wavelength of the X-ray is 0.144556 nm, B is the width at half maximum of the diffraction peak, θ is the Bragg angle, d is the interplanar spacing, and the calculated values in Table 4 are derived from the (111) diffraction peaks.

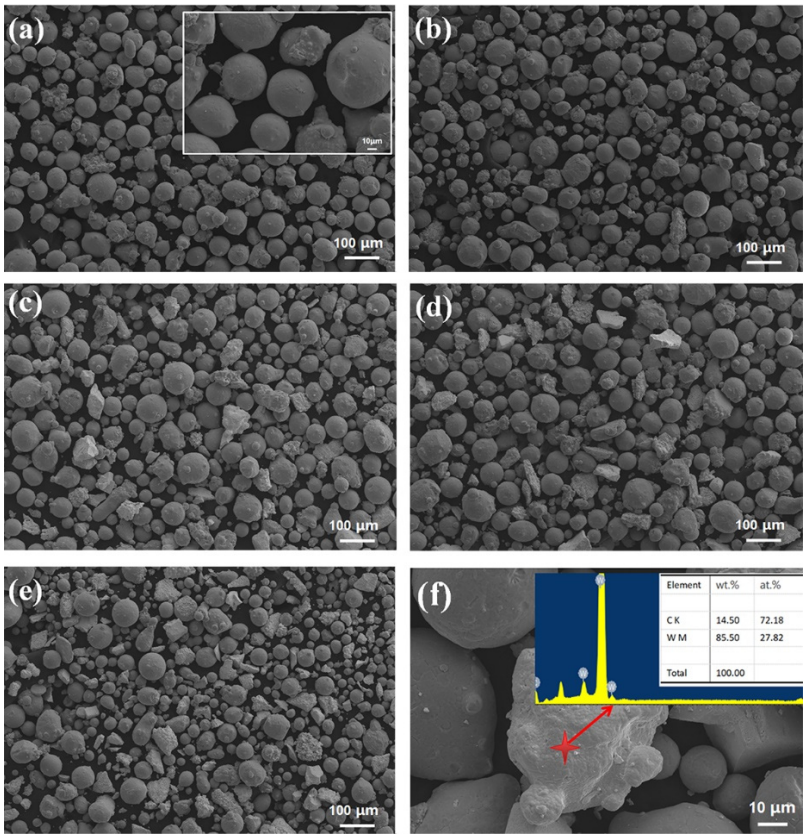

Figure 2. SEM images and EDS spectra of mixed powders: (**a**) CoCrFeNi; (**b**) CoCrFeNi+10 wt.%WC; (**c**) CoCrFeNi+20 wt.%WC; (**d**) CoCrFeNi+30 wt.%WC; (**e**) CoCrFeNi+40 wt.%WC; (**f**) EDS spectra of irregular WC particles.

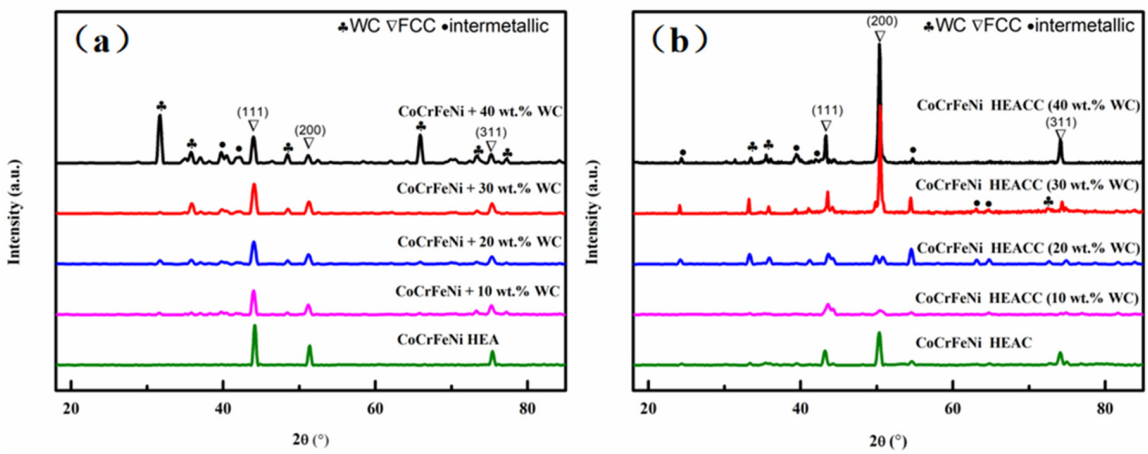

Figure 3. XRD patterns: (**a**) mixed powders; (**b**) CoCrFeNi HEACC.

Table 4. Crystallite size (D) and lattice constant (a) of the FCC phase (111) peak in coatings.

Coatings	D (nm)	a (Å)
CoCrFeNi HEAC	35.8	1.892
CoCrFeNi HEACC (10 wt.% WC)	20.8	3.225
CoCrFeNi HEACC (20 wt.%WC)	15.5	3.575
CoCrFeNi HEACC (30 wt.% WC)	19.6	3.116
CoCrFeNi HEACC + (40 wt.% WC)	30.4	2.115

The calculated lattice constant (a) and grain size (D) of the particle were plotted as curves to facilitate observation of the rules. As can be seen from Figure 4, as the addition of WC is increased, the grain size initially decreases and then increases whereas the lattice constant initially increases and then decreases. From the change in lattice constant, it is clear that the addition of WC consists of unmelted particles and intermetallic compounds, as well as a small portion of WC that will enter the FCC lattice and form a solid solution, thereby causing lattice distortion of CoCrFeNi HEAC [42]. This will enhance the effect of strengthening solid solutions. However, when the WC content is higher than 20 wt.%, the lattice distortion decreases. This may be because the solubility of the FCC lattice tends to be saturated and a large number of WC particles fail to melt during the rapid melting process of laser cladding, resulting in unmelted particles that delay the entry of the FCC lattice into the material. The change in grain size also indicates that WC contributes to the grain refinement of CoCrFeNi HEAC. The addition of WC particles may result in two reasons for grain refinement. It is true that WC tends to be found at the grain boundary of FCC during the melting process, and WC at the grain boundary helps to strengthen the grain boundary and prevent it from expanding. In contrast, grain size increases when WC is greater than 20 wt.%, which may be due to the fact that WC begins to gather at some locations and is no longer distributed along grain boundaries. As a result, it can be concluded that when the WC level is higher than 20 wt.%, the solubility of the FCC matrix begins to decline and aggregates into unmelted particles. From the perspective of structure, according to the effect of solution strengthening, fine grain strengthening, and dispersion strengthening, it can be concluded that mechanical properties are optimal with WC content slightly above 20 wt.%.

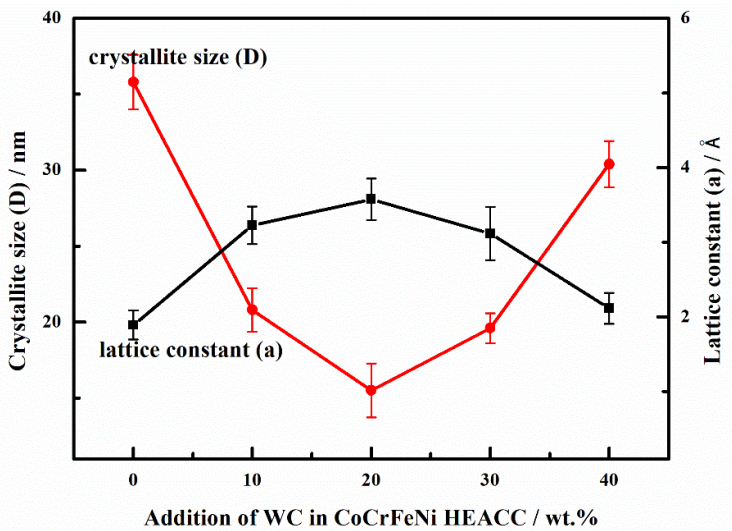

Figure 4. The grain size (D) and lattice constant (a) of the FCC phase in CoCrFeNi HEACC with increasing WC addition.

Figure 5 illustrates the backscatter image of the coatings specimen. As shown in the Figure 5a–d, there is a transition zone between the coating and the substrate. With the addition of WC, the transition zone expands and is typically located between 10 and 20 μm. It is evident that the bonding surface between the CoCrFeNi HEACC and the matrix is relatively smooth when the WC content is less than 40 wt.%, indicating that both CoCrFeNi HEACC and substrate are mutually soluble to ensure good bonding.

Figure 6 illustrates the local magnification of the backscatter images of the coatings specimen. Accordingly, it is evident from the figure that when WC was added, bright white dendrites appeared in the coating (Figure 6a,b), further increased after the addition of 20–30 wt.% WC (Figure 6c,d), and finally formed a eutectic mixture with the HEA matrix after 40 wt.% WC was added (Figure 6e). When adding excess WC in the coating, the area of the diffusion layer became larger. This may be due to the large amount of WC melting

at a higher temperature making the element diffuse in the molten pool when the mobile laser power is used for cladding. In turn, the coating becomes more uniform. In addition, it can be clearly seen in Figure 5e that there are a large number of cracks and holes in the coating, and there are fluctuations in the bonding surface, which are related to the higher energy required by excessive WC melting. It is also necessary to redesign the laser power and other parameters to minimize the effects of excessive WC on molten pool morphology.

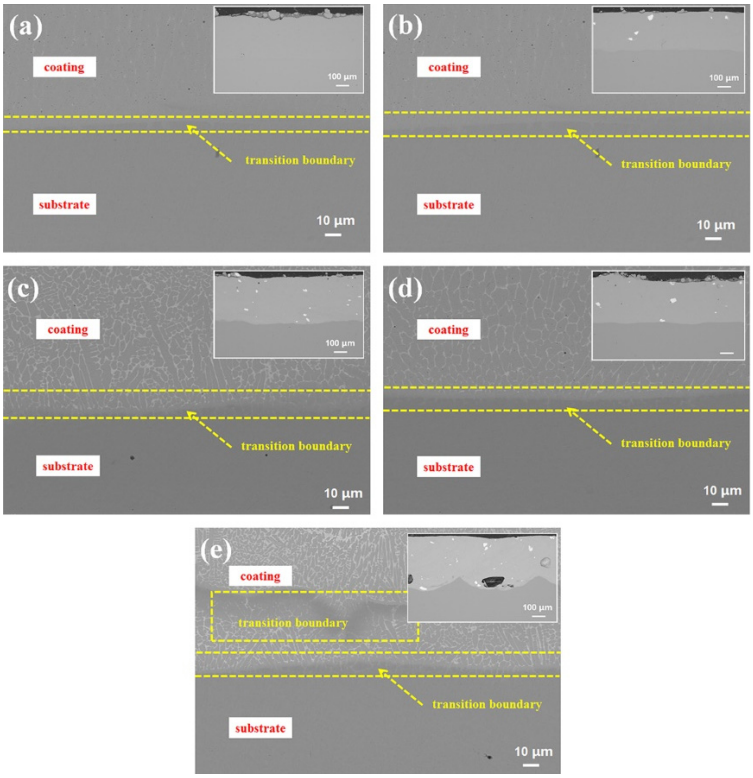

Figure 5. Cross-sectional FESEM images of coatings: (**a**) CoCrFeNi HEAC; (**b**) CoCrFeNi HEACC (10 wt.% WC); (**c**) CoCrFeNi HEACC (20 wt.% WC); (**d**) CoCrFeNi HEACC (30 wt.% WC); (**e**) CoCrFeNi HEACC (40 wt.% WC).

In order to further confirm the composition of these dendritic eutectic compounds, EDS results indicate that these compounds are intermetallic compounds that contain W, as shown in Figure 6f. According to the speculation, when adding a small amount of WC, it will dissolve the priority in the process of laser cladding and the CoCrFeNi HEACC to form a solid solution. In addition, an increase in WC mass addition will result in precipitation of the W element from intermetallic compounds, resulting in a eutectic mixture. In addition, large white and bright particles with a diameter of a few tens of microns are also visible in Figure 5. Figure 7 shows the distribution of white and bright particles on the surface of CoCrFeNi HEACC as determined by EDS mapping. It should be pointed out that element C, as a relatively light element, cannot be accurately measured under our current testing conditions (EDS elemental surface distribution test), so the element C surface distribution in Figure 7 has some inaccuracy. Nevertheless, based on the distribution of other elements, we can conclude that the bright white particles are unmelted WC particles. So, we can speculate that under high energy laser irradiation, a portion of the WC particles dissolve and form a solid solution with high entropy alloy, a portion forms W-rich intermetallic compounds, and the remainder is retained within the matrix, due to a short residence time in the high-temperature region.

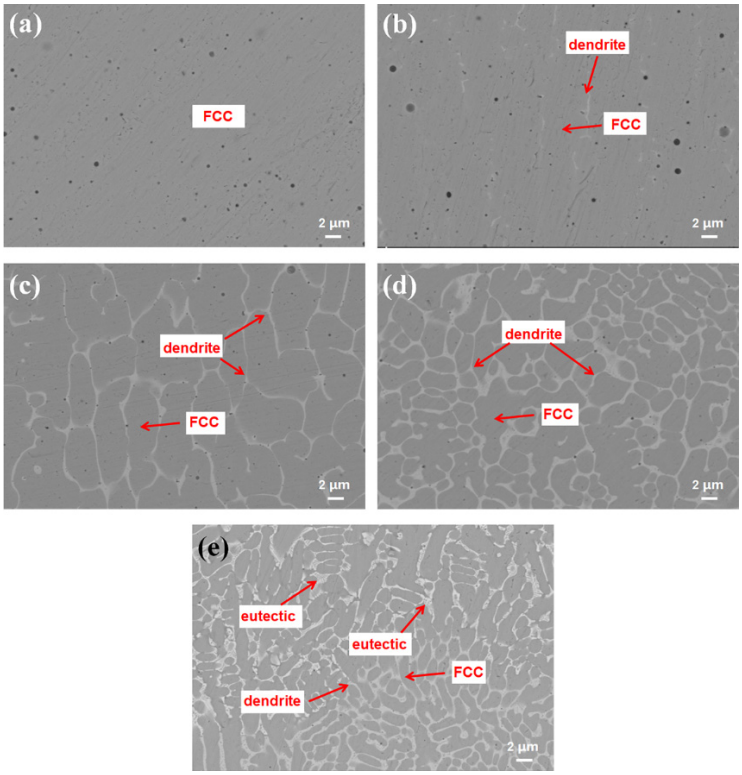

Figure 6. Local magnification FESEM images of coatings: (**a**) CoCrFeNi HEAC; (**b**) CoCrFeNi HEACC (10 wt.% WC); (**c**) CoCrFeNi HEACC (20 wt.% WC); (**d**) CoCrFeNi HEACC (30 wt.% WC); (**e**) CoCrFeNi HEACC (40 wt.% WC).

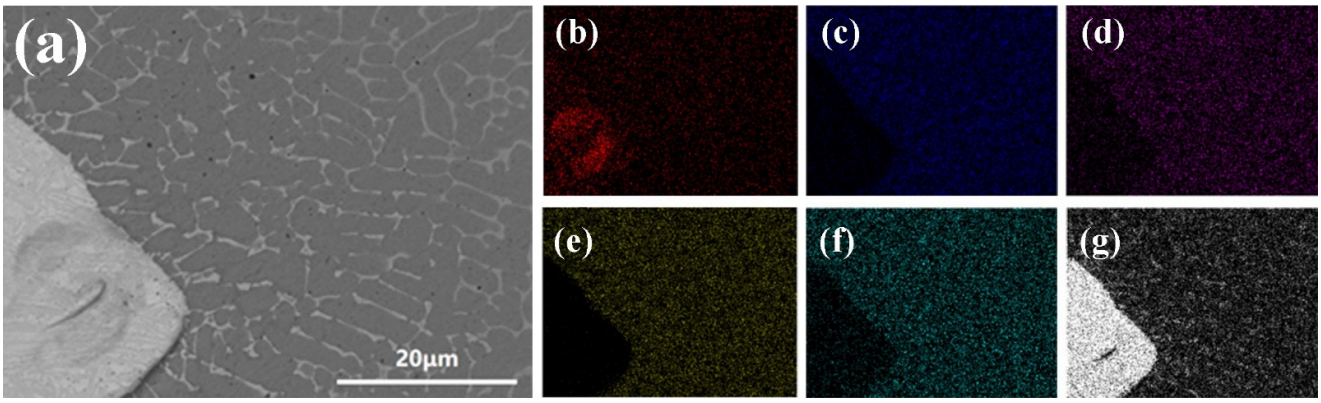

Figure 7. EDS element mapping of CoCrFeNi HEACC (40 wt.% WC). (**a**) SEM image of CoCrFeNi HEACC (40 wt.% WC); EDS element mapping of CoCrFeNi HEACC (40 wt.% WC): (**b**) C; (**c**) Cr; (**d**) Ni; (**e**) Fe; (**f**) Co; (**g**) W.

Figure 8 illustrates the morphology of cracks and holes in order to provide a better understanding of these phenomena. Based on the FESEM results, it is obvious that the semi-arc crack in the coating is typical of liquefaction cracks, which are formed when the eutectic at the grain boundary is remelted during the laser cladding process, resulting in inner granular cracking related to shrinkage, and finally bending and expanding [43,44]. The hole in the coating is caused by the poor adhesion between excessive WC particles and the CoCrFeNi HEACC, which causes the particles to fall off during the metallographic preparation process.

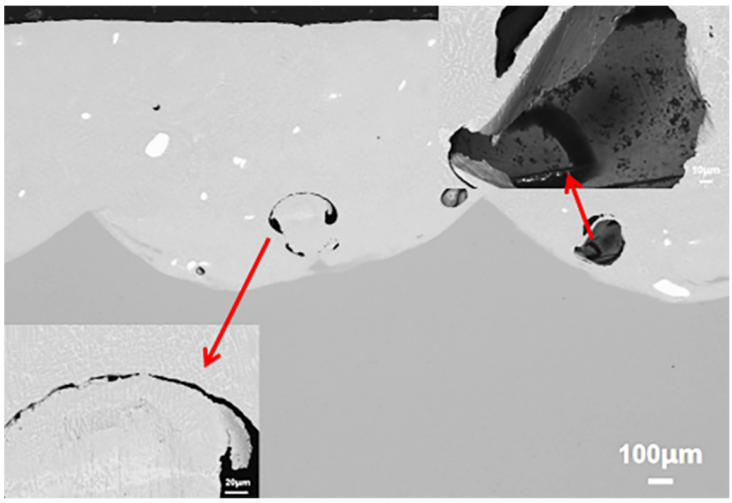

Figure 8. The cracks and holes in FESEM image of CoCrFeNi HEACC (40 wt.% WC).

3.2. Wear Resistance

A weight loss chart of the CoCrFeNi HEACC during friction and wear can be found in Figure 9. It is evident that, with the addition of WC, the CoCrFeNi HEACC 's wear resistance improves, but excessive WC (40 wt.%) will deteriorate the CoCrFeNi HEACC's wear resistance. Based on the previous analysis, CoCrFeNi HEA has extremely low wear resistance due to its single-phase FCC structure. Adding WC to CoCrFeNi HEA produces two effects: It strengthens the matrix in the solid solution and, in addition, it precipitates out w-rich intermetallic compounds that allow the coating to be strengthened, leading to improvements in wear resistance of 20–30 wt.%. It is consistent with the previous prediction analysis. When excessive amounts of WC are added, a large proportion of unmelted WC and a large proportion of eutectic materials greatly enhance the brittleness of the coating, culminating in residual stresses and micropores during the laser cladding process, which have a detrimental effect on the CoCrFeNi HEACC's wear resistance. Moreover, the increase in grain size and the reduction of lattice distortion in Figure 4. This may also explain the lower wear resistance of the CoCrFeNi HEACC.

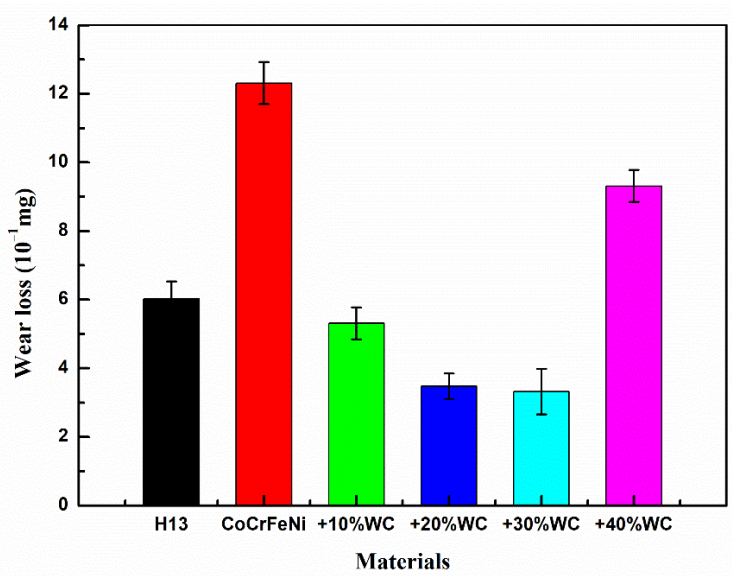

Figure 9. The wear mass loss of coatings: H13 (black); CoCrFeNi HEAC (red); CoCrFeNi HEACC (10 wt.% WC: green); CoCrFeNi HEACC (20 wt.% WC: blue); CoCrFeNi HEACC (30 wt.% WC: cyan); CoCrFeNi HEACC (40 wt.% WC: purple).

In order to further analyze the wear failure behavior of the CoCrFeNi HEACC, Figure 10 shows the FESEM images of the bottom of the wear trace of laser cladding CoCrFeNi HEACC after friction and wear. The results show that CoCrFeNi HEAC has a high plasticity without WC, so plastic deformation occurs in the CoCrFeNi HEAC area when it is extruded by the grinding head and forms a plastic deformation area. Currently, adhesive wear is the predominant form of CoCrFeNi HEAC. There are obvious layers of peeling in the CoCrFeNi HEAC, this is due to the rapid cooling of the CoCrFeNi HEAC after the laser cladding, friction stress, and shear stress in the process of friction are prone to stress concentration, resulting in the development of micro cracks. These micro cracks are generated during friction stress in the crack propagation, which in turn forms the layered peeling coating, as shown in Figure 10a. It is still true that the above phenomenon occurs when 10 wt.% WC is added, as shown in Figure 10b. When the WC addition amount is 20 wt.%, as shown in Figure 10c, delamination is significantly reduced. WC on the one hand induces a solid solution strengthening of the CoCrFeNi HEAC matrix while on the other hand, a large number of w-rich intermetallic dendrites also influence the strengthening of the CoCrFeNi HEAC matrix, leading to the change of the wear form of the CoCrFeNi HEACC to abrasive wear. When the WC addition amount is 30 wt.%, as shown in Figure 10d, the worn surface becomes smooth, no delamination and plastic deformation are found, and WC particles are well retained, only a small amount of local fragmentation occurs. As a result, the CoCrFeNi HEAC has shown good plastic deformation resistance under repeated cutting and extrusion of Si_3N_4 balls during friction, which is consistent with the lowest weight loss obtained in Figure 9. Further increases in the WC content to 40 wt.% result in delamination and thousands of cracks in the CoCrFeNi HEAC, as shown in Figure 10e, and wear resistance is significantly reduced. At the present time, the decrease in the amount of high-entropy plastic matrix in the CoCrFeNi HEACC results in fewer WC particles adhering to the matrix in the CoCrFeNi HEACC with friction, resulting in a large number of WC particles shedding from the matrix coating. An excessive amount of WC can also lead to the formation of brittle eutectic substances in high entropy matrixes, and the development of cracks under the influence of external forces can be expected. Furthermore, due to the large difference in the thermal expansion coefficient between the CoCrFeNi HEA matrix and WC, significant thermal stresses will be generated during the rapid cooling process of laser cladding. In addition, an excessive amount of eutectic mixture can increase the brittleness of the CoCrFeNi HEA matrix, resulting in numerous microcracks in the CoCrFeNi HEACC. The experience of external loads produced a concentration of stresses near the crack, which accelerated crack propagation and significantly enhanced the wear rate of the CoCrFeNi HEACC.

3.3. Corrosion Resistance

The corrosion of metal components in aqueous solution involves the anodic dissolution of metals as well as the cathodic reduction of oxidants [45]. Under open circuit conditions or with the application of a small potential, the sample's composition slowly and selectively disintegrates, but when a relatively high potential is applied or at a relatively high potential range, significant dissolution will take place on the coating's surface [46]. The corrosion process of the tested samples must be observed and studied through polarization curves in order to identify the effect of WC on the corrosion behavior of high entropy alloys. Figure 11 shows the polarization curve for CoCrFeNi HEACC (WC content from 0~40 wt.%) in 3.5 wt.% NaCl solution. During electrochemical corrosion conditions, the test sample's corrosion potential (E_{corr}) and corrosion current density (i_{corr}) were calculated. Passivation occurs more frequently at lower corrosion current densities, the passivation film forms faster, and the formation of the passivation film prevents the inner layer from being exposed to corrosive fluids, thus slowing the corrosion reaction [47,48]. Electrochemical parameters of CoCrFeNi HEACC are shown in Table 5. As illustrated in Figure 11, with the addition of WC, the E_{corr} and i_{corr} are similar, indicating that WC has little influence on the corrosion resistance of CoCrFeNi HEACC. However, careful observation of the corrosion potentials

for the coatings reveals that with the increase of the WC addition amount, the corrosion potential shows a slight decreasing trend, indicating that the addition of WC will reduce the corrosion resistance. This may be due to the fact that the addition of WC makes intermetallic compounds, eutectic mixtures and other multiphase structures appear in the high-entropy FCC coating, causing corrosion cells and resulting in a reduction in corrosion resistance.

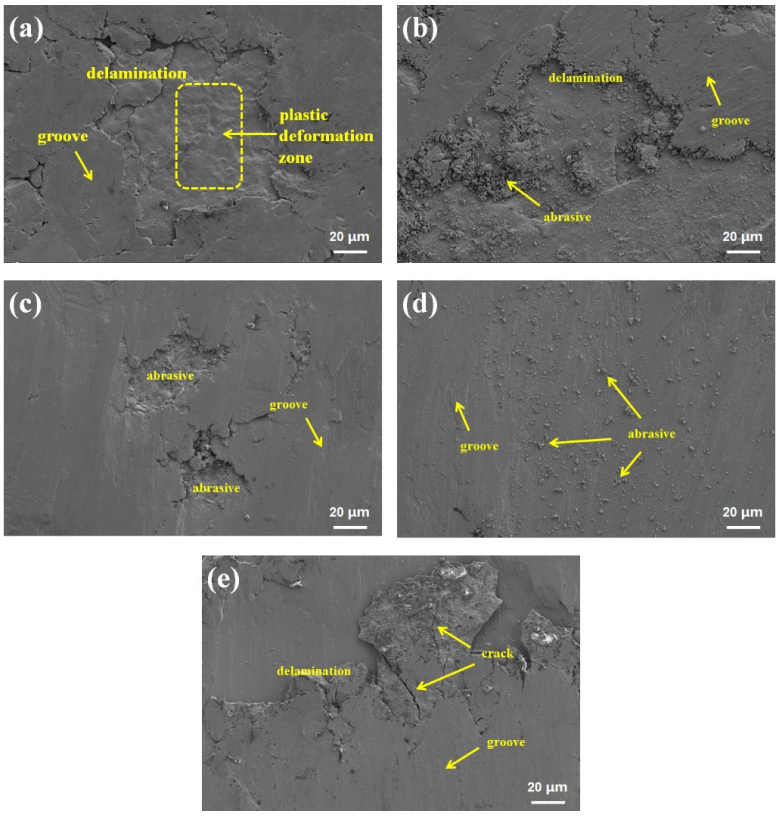

Figure 10. FESEM images of coatings after wear: (**a**) CoCrFeNi HEAC; (**b**) CoCrFeNi HEACC (10 wt.% WC); (**c**) CoCrFeNi HEACC (20 wt.% WC); (**d**) CoCrFeNi (30 wt.% WC); (**e**) CoCrFeNi HEACC (40 wt.% WC).

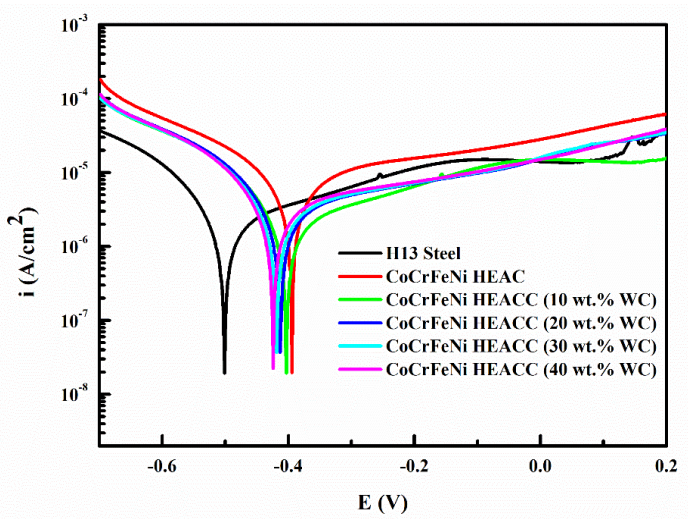

Figure 11. Polarization curve of H13 steel substrate (black) and coatings on H13 steel: CoCrFeNi HEAC (red); CoCrFeNi HEACC (10 wt.% WC: green); CoCrFeNi HEACC (20 wt.% WC: blue); CoCrFeNi (30 wt.%WC: cyan); CoCrFeNi HEACC (40 wt.% WC: purple).

Table 5. Corrosion dynamics parameters for the materials.

Materials	E_{corr}/V	i_{corr}/(A·cm^{-2})
H13 Steel	−0.501	2.66×10^{-7}
CoCrFeNi HEAC	−0.394	3.52×10^{-7}
CoCrFeNi HEACC (10 wt.% WC)	−0.403	2.76×10^{-7}
CoCrFeNi HEACC (20 wt.% WC)	−0.413	2.97×10^{-7}
CoCrFeNi HEACC (30 wt.% WC)	−0.418	2.99×10^{-7}
CoCrFeNi HEACC (40 wt.% WC)	−0.424	2.89×10^{-6}

4. Conclusions

In this study, CoCrFeNi HEACC (0, 10 wt.%, 20 wt.%, 30 wt.%, and 40 wt.%, respectively) were prepared on H13 substrates by laser cladding. The influence of WC on the microstructure, structure, wear resistance, corrosion resistance and wear resistance of CoCrFeNi HEACC were investigated, and the conclusions could be drawn as follows:

(1) Under the high energy of the laser, a large number of WC will decompose and dissolve in the FCC matrix phase, and the coating will gradually change from a single-phase structure of FCC to a multi-phase structure of FCC + intermetallic compound + unmelted WC, and the lattice distortion of the FCC matrix phase will also increase with the addition of WC. An excessive amount of WC may cause a large number of unmelted particles to appear in the CoCrFeNi HEACC, and WC dissolving in the FCC matrix will tend to become saturated. During this period, the lattice distortion of the FCC matrix phase decreases. In addition, a large number of segregation, cracks, and other defects will appear in the CoCrFeNi HEACC;

(2) With the addition of WC, the wear resistance of CoCrFeNi HEACC at room temperature increases first and then decreases, reaching an optimal value within the range of 20–30 wt.%, which is consistent with the analysis of the CoCrFeNi HEACC structure. The presence of WC dissolved in the FCC matrix phase as well as intermetallic compounds precipitated as dendrites can strengthen the CoCrFeNi HEACC; however, an excessive amount of WC will result in numerous defects and brittle eutectic in the CoCrFeNi HEACC, effectively reducing its wear resistance;

(3) The corrosion potential (E_{corr}) and corrosion current density (I_{corr}) of CoCrFeNi CoCrFeNi HEACC are nearly similar after the addition of WC, and the corrosion potential shows a slight decrease, which indicates that WC has little impact on corrosion resistance.

Author Contributions: The idea was proposed by T.W., Y.C., Y.W. and J.L. The experiments were carried out by T.W., B.L. and L.Y. The experimental results were analyzed and interpreted by T.W. and W.G., T.W. and W.G. wrote the main manuscript text. The manuscript was reviewed and further analyzed by T.W., W.G. and D.Z. All authors have read and agreed to the published version of the manuscript.

Funding: This research was funded by Zhejiang Provincial Key R&D Program: (No. 2022C01147); Zhejiang Provincial Natural Science Foundation (No. LGG21E010005); State Key Lab of Advanced Metals and Materials (No. 2020-Z07, 2021-ZD01); State Key Laboratory of Materials Processing and Die & Mould Technology, Huazhong University of Science and Technology (No. P2022-026); National Natural Science Foundation of China (No. 52101070); National Key Research and Development Program of China (No. 2021YFB3700503).

Institutional Review Board Statement: Not applicable.

Informed Consent Statement: Not applicable.

Data Availability Statement: The data that support the findings of this study are available from the corresponding author upon reasonable request.

Conflicts of Interest: The authors declare no conflict of interest.

References

1. Tan, Q.Y.; Yin, Y.; Wang, F.; Chang, H.W.; Liu, S.Y.; Liang, G.F.; Wu, T.; Zhang, M.X. Rationalization of brittleness and anisotropic mechanical properties of H13 steel fabricated by selective laser melting. *Scr. Mater.* **2022**, *214*, 114645. [CrossRef]
2. Yuan, M.W.; Cao, Y.; Karamchedu, S.; Hosseini, S.; Yao, Y.M.; Berglund, J.; Liu, L.B.; Nyborg, L. Characteristics of a modified H13 hot-work tool steel fabricated by means of laser beam powder bed fusion. *Mater. Sci. Eng. A-Struct.* **2022**, *831*, 142322. [CrossRef]
3. Navid, A.; Maryam, M.; Kazem, B.; Arash, F.A. New promising ceramic coatings for corrosion and wear protection of steels: A review. *Surf. Interfaces* **2021**, *23*, 100997.
4. Li, X.; Zhang, C.H.; Zhang, S.; Wu, C.L.; Liu, Y.; Zhang, J.B.; Shahzad, M.B. Manufacturing of Ti3SiC2 lubricated Co-based alloy coatings using laser cladding technology. *Opt. Laser Technol.* **2019**, *114*, 209. [CrossRef]
5. Yuan, W.Y.; Li, R.F.; Chen, Z.H.; Gu, J.Y.; Tian, Y.T. A comparative study on microstructure and properties of traditional laser cladding and high-speed laser cladding of Ni45 alloy coatings. *Surf. Coat. Technol.* **2021**, *405*, 126582. [CrossRef]
6. Shen, F.M.; Tao, W.; Li, L.Q.; Zhou, Y.D.; Wang, W.; Wang, S.L. Effect of microstructure on the corrosion resistance of coatings by extreme high speed laser cladding. *Appl. Surf. Sci.* **2020**, *517*, 146085. [CrossRef]
7. Schopphoven, T.; Gasser, A.; Wissenbach, K.; Poprawe, R. Investigation on ultra-high-speed laser material deposition as alternative for hard chrome plating and thermal spraying. *J. Laser Appl.* **2016**, *28*, 002501. [CrossRef]
8. Gui, W.Y.; Zhong, C.; Gu, J.Y.; Ding, Y.H.; Wang, X.M.; Wu, T.; Liang, Y.F.; Qin, J.Y.; Qu, Y.H.; Lin, J.P. Laser-clad Inconel 625 coatings on Q245R structure steel: Microstructure, wear and corrosion resistance. *npj Mater Degrad.* **2022**, *6*, 37. [CrossRef]
9. Zhang, Y.; Zuo, T.T.; Tang, Z.; Gao, M.C.; Dahmen, K.A.; Liaw, P.K.; Lu, Z.P. Microstructures and properties of high-entropy alloys. *Prog. Mater. Sci.* **2014**, *61*, 1–93. [CrossRef]
10. Yeh, J.W.; Chen, S.K.; Lin, S.J.; Gan, G.Y.; Chin, T.S.; Shun, T.T.; Tsau, C.H.; Chang, S.Y. Nanostructured high-entropy alloys with multiple principal elements: Novel alloy design concepts and outcomes. *Adv. Eng. Mater.* **2004**, *6*, 299. [CrossRef]
11. Luo, H.; Li, Z.; Mingers, A.M.; Raabe, D. Corrosion behavior of an equiatomic CoCrFeMnNi high-entropy alloy compared with 304 stainless steel in sulfuric acid solution. *Corros. Sci.* **2018**, *134*, 131. [CrossRef]
12. Wu, T.; Chen, Y.X.; Shi, S.Q.; Wu, M.T.; Gui, W.Y.; Tan, Y.Y.; Li, J.H.; Wu, Y. Effects of W Alloying on the Lattice Distortion and Wear Behavior of Laser Cladding AlCoCrFeNiWx High-Entropy Alloy Coatings. *Materials* **2021**, *14*, 5450. [CrossRef] [PubMed]
13. Liu, J.; Liu, H.; Chen, P.J.; Hao, J.B. Microstructural characterization and corrosion behaviour of AlCoCrFeNiTix high-entropy alloy coatings fabricated by laser cladding. *Surf. Coat. Technol.* **2019**, *361*, 63. [CrossRef]
14. Shang, C.Y.; Axinte, E.; Sun, J.; Li, X.T.; Li, P.; Du, J.W.; Qiao, P.C.; Wang, Y. CoCrFeNi(W1−xMox) high-entropy alloy coatings with excellent mechanical properties and corrosion resistance prepared by mechanical alloying and hot pressing sintering. *Mater. Des.* **2017**, *117*, 193. [CrossRef]
15. Li, X.F.; Feng, Y.H.; Liu, B.; Yi, D.H.; Yang, X.H.; Zhang, W.D.; Chen, G.; Liu, Y.; Bai, P.K. Influence of NbC particles on microstructure and mechanical properties of AlCoCrFeNi high-entropy alloy coatings prepared by laser cladding. *J. Alloys Compd.* **2019**, *788*, 485. [CrossRef]
16. Fu, Y.; Huang, C.; Du, C.W.; Li, J.; Dai, C.D.; Luo, H.; Liu, Z.Y.; Li, X.G. Evolution in microstructure, wear, corrosion, and tribocorrosion behavior of Mo-containing high-entropy alloy coatings fabricated by laser cladding. *Corros. Sci.* **2021**, *191*, 109727. [CrossRef]
17. Jayaraj, J.; Thinaharan, C.; Ningshen, S.; Mallika, C.; Mudali, U.K. Corrosion behavior and surface film characterization of TaNbHfZrTi high entropy alloy in aggressive nitric acid medium. *Intermetallics* **2017**, *89*, 123. [CrossRef]
18. Vallimanalan, A.; Babu, S.P.K.; Muthukumaran, S.; Murali, M.; Gaurav, V.; Mahendran, R. Corrosion behaviour of thermally sprayed Mo added AlCoCrNi high entropy alloy coating. *Mater. Today Proc.* **2020**, *27*, 2398. [CrossRef]
19. Liu, Y.Y.; Chen, Z.; Shi, J.C.; Wang, Z.Y.; Zhang, J.Y. The effect of Al content on microstructures and comprehensive properties in AlxCoCrCuFeNi high entropy alloys. *Vacuum* **2019**, *161*, 143. [CrossRef]
20. Dai, C.D.; Luo, H.; Li, J.; Du, C.W.; Liu, Z.Y.; Yao, J.Z. X-ray photoelectron spectroscopy and electrochemical investigation of the passive behavior of high-entropy FeCoCrNiMox alloys in sulfuric acid. *Appl. Surf. Sci.* **2020**, *499*, 143903. [CrossRef]
21. Xiao, D.H.; Zhou, P.F.; Wu, W.Q.; Diao, H.Y.; Gao, M.C.; Song, M.; Liaw, P.K. Microstructure, mechanical and corrosion behaviors of AlCoCuFeNi-(Cr, Ti) high entropy alloys. *Mater. Des.* **2017**, *116*, 438. [CrossRef]
22. Medina, L.Z.; Riekehr, L.; Jansson, U. Phase formation in magnetron sputtered CrMnFeCoNi high entropy alloy. *Surf. Coat. Technol.* **2020**, *403*, 126323. [CrossRef]
23. Wang, L.M.; Chen, C.C.; Yeh, J.W.; Ke, S.T. The microstructure and strengthening mechanism of thermal spray coating NixCo0.6Fe0.2CrySizAlTi0.2 high-entropy alloys. *Mater. Chem. Phys.* **2011**, *126*, 880. [CrossRef]
24. Cai, Z.B.; Wang, Y.D.; Cui, X.F.; Jin, G.; Li, Y.; Liu, Z.; Dong, M.L. Design and microstructure characterization of FeCoNiAlCu high-entropyalloy coating by plasma cladding: In comparison with thermodynamic calculation. *Surf. Coat. Technol.* **2017**, *330*, 163. [CrossRef]
25. Zhang, S.Y.; Han, B.; Li, M.Y.; Zhang, Q.; Hu, C.Y.; Niu, S.Y.; Li, Z.H.; Wang, Y. Investigation on solid particles erosion resistance of laser cladded CoCrFeNiTi high entropy alloy coating. *Intermetallics* **2021**, *131*, 107111. [CrossRef]
26. Guo, Y.J.; Li, C.G.; Zeng, M.; Wang, J.Q.; Wang, Y. In-situ TiC reinforced CoCrCuFeNiSi0.2 high-entropy alloy coatings designed for enhanced wear performance by laser cladding. *Mater. Chem. Phys.* **2020**, *242*, 122522. [CrossRef]
27. Cheng, J.B.; Liu, D.; Liang, X.B.; Chen, Y.X. Evolution of microstructure and mechanical properties of in situ synthesized TiC-TiB_2/CoCrCuFeNi high entropy alloy coatings. *Surf. Coat. Technol.* **2015**, *281*, 109. [CrossRef]

28. Xu, J.; Wang, S.R.; Shang, C.Y.; Huang, S.F.; Wang, Y. Microstructure and properties of CoCrFeNi (WC) high-entropy alloy coatings prepared using mechanical alloying and hot pressing sintering. *Coatings* **2019**, *9*, 16. [CrossRef]
29. Liu, H.; Liu, J.; Chen, P.J.; Yang, H.F. Microstructure and high temperature wear behaviour of in-situ TiC reinforced AlCoCrFeNi-based high-entropy alloy composite coatings fabricated by laser cladding. *Opt. Laser. Technol.* **2019**, *118*, 140. [CrossRef]
30. Wang, Z.W.; Baker, I.; Cai, Z.H.; Chen, S.; Poplawsky, J.D.; Guo, W. The effect of interstitial carbon on the mechanical properties and dislocation substructure evolution in Fe40.4Ni11.3Mn34.8Al7.5Cr6 high entropy alloys. *Acta Mater.* **2016**, *120*, 228. [CrossRef]
31. Ji, X.L.; Zhao, J.H.; Wang, H.; Luo, C.Y. Sliding wear of spark plasma sintered CrFeCoNiCu high entropy alloy coatings with MoS_2 and WC additions. *Int. J. Adv. Manuf. Technol.* **2018**, *96*, 1685. [CrossRef]
32. Dong, D.Q.; Xiang, X.; Huang, B.; Xiong, H.W.; Zhang, L.; Shi, K.H.; Liao, J. Microstructure and properties of WC-Co/CrMnFeCoNi composite cemented carbides. *Vacuum* **2020**, *179*, 109571. [CrossRef]
33. Liu, Y.; Xu, T.H.; Liu, Y.; Gao, Y.L.; Di, C. Wear and heat shock resistance of Ni-WC coating on mould copper plate fabricated by laser. *J. Mater. Res. Technol.* **2020**, *9*, 8283. [CrossRef]
34. Wei, L.; Liu, Y.; Li, Q.; Cheng, Y.F. Effect of roughness on general corrosion and pitting of $(FeCoCrNi)_{0.89}(WC)_{0.11}$ high-entropy alloy composite in 3.5% NaCl solution. *Corros. Sci.* **2019**, *146*, 44. [CrossRef]
35. Li, D.Y.; Jiang, H.; Zou, L.J.; Cao, Z.Q. Effects of WC content on microstructure and properties of laser cladding $AlCoCrFeNiNb_{0.75}$ high-entropy alloy coating. *Hot Work. Technol.* **2019**, *48*, 117.
36. Li, J.; Xiang, S.; Luan, H. Additive manufacturing of high-strength CrMnFeCoNi high-entropy alloys-based composites with WC addition. *J. Mater. Sci. Technol.* **2019**, *35*, 2430. [CrossRef]
37. Luo, W.Y.; Liu, Y.Z.; Shen, J.J. Effects of binders on the microstructures and mechanical properties of ultrafine WC-10%AlxCoCrCuFeNi composites by spark plasma sintering. *J. Alloys Compd.* **2019**, *791*, 540. [CrossRef]
38. Peng, Y.B.; Zhang, W.; Li, T.C.; Zhang, M.Y.; Wang, L.; Song, Y.; Hu, S.H.; Hu, Y. Microstructures and mechanical properties of FeCoCrNi high entropy alloy/WC reinforcing particles composite coatings prepared by laser cladding and plasma cladding. *Int. J. Refract. Met. Hard Mater.* **2019**, *84*, 105044. [CrossRef]
39. Angelo, F.A.; Olga, S.; Victor, T.W.; Andreoli, A.F.; Shuleshova, O.; Witusiewicz, V.T.; Wu, Y.H.; Yang, Y.Z.; Ivashko, O.; Dippel, A.C.; et al. In situ study of non-equilibrium solidification of CoCrFeNi high-entropy alloy and CrFeNi and CoCrNi ternary suballoys. *Acta Mater.* **2021**, *212*, 116880.
40. Shang, C.Y.; Axinte, E.; Ge, W.J.; Zhang, Z.T.; Wang, Y. High-entropy alloy coatings with excellent mechanical, corrosion resistance and magnetic properties prepared by mechanical alloying and hot pressing sintering. *Surf. Interfaces* **2017**, *9*, 36. [CrossRef]
41. Peng, Y.B.; Zhang, W.; Li, T.C.; Zhang, M.Y.; Liu, B.; Liu, Y.; Wang, L.; Hu, S.H. Effect of WC content on microstructures and mechanical properties of FeCoCrNi high-entropy alloy/WC composite coatings by plasma cladding. *Surf. Coat. Technol.* **2020**, *385*, 125326. [CrossRef]
42. Tan, Y.Y.; Chen, Z.J.; Su, M.Y.; Ding, G.; Jiang, M.Q.; Xie, Z.C.; Gong, Y.; Wu, T.; Wu, Z.H.; Wang, H.Y.; et al. Lattice distortion and magnetic property of high entropy alloys at low temperatures. *J. Mater. Sci. Technol.* **2022**, *104*, 236. [CrossRef]
43. Bian, H.Y.; Zhai, X.Y.; Wang, S.J.; Li, Y.; Wang, W. Influence of Heat Input and Thermal Cycling on the Crack and Microstructure of Laser Deposition Repair DZ125 Alloy. *Rare Metal Mater. Eng.* **2020**, *49*, 1702.
44. Brennan, M.C.; Keist, J.S.; Palmer, T.A. Defects in Metal Additive Manufacturing Processes. *J. Mater. Eng. Perform.* **2021**, *30*, 4808. [CrossRef]
45. Da Silva, F.S.; Cinca, N.; Dosta, S.; Cano, I.G.; Couto, M.; Guilemany, J.M.; Benedetti, A.V. Corrosion behavior of WC-Co coatings deposited by cold gas spray onto AA 7075-T6. *Corros. Sci.* **2018**, *136*, 231. [CrossRef]
46. Ge, W.J.; Li, B.; Axinte, E.; Zhang, Z.T.; Shang, C.Y.; Wang, Y. Crystallization and corrosion resistance in different aqueous solutions of Zr50.7Ni28Cu9Al12.3 amorphous alloy and its crystallization counterparts. *JOM* **2017**, *69*, 776. [CrossRef]
47. Chen, Y.Y.; Duval, T.; Hung, U.D.; Yeh, J.W.; Shih, H.C. Microstructure and electrochemical properties of high entropy alloys–A comparison with type-304 stainless steel. *Corros. Sci.* **2005**, *47*, 2257. [CrossRef]
48. Gan, Y.; Wang, W.X.; Guan, Z.S.; Cui, Z.Q. Multi-layer laser solid forming of Zr65Al7.5Ni10Cu17.5 amorphous coating: Microstructure and corrosion resistance. *Opt. Laser Technol.* **2015**, *69*, 17. [CrossRef]